Measurement of prompt fission neutron spectrum for spontaneous fission of ^{252}Cf using γ multiplicity tagging

E. Blain,* A. Daskalakis, R. C. Block, and Y. Danon
Gaerttner LINAC Center, Rensselaer Polytechnic Institute, Troy, New York 12180, USA
(Received 27 May 2016; revised manuscript received 22 May 2017; published 30 June 2017)

The prompt fission neutron spectrum from spontaneous fission of ^{252}Cf is an integral part of several aspects of nuclear data. Not only is the spectrum itself of interest, but neutron detectors often use the spectrum for calibration, and other prompt fission neutron spectra are measured as a ratio to ^{252}Cf. Therefore, reducing the uncertainties in this spectrum will allow for more accurate nuclear data to be available across a wide range of fields. The prompt fission neutron spectrum for the spontaneous fission of ^{252}Cf was measured at Rensselaer Polytechnic Institute using the multiple γ tagging method with a 18.4-ng fission sample. An EJ-301 liquid scintillator fast neutron detector was used to measure the high energy portion of the spectrum, 0.5–7 MeV, and a thin EJ-204 plastic scintillator was used to measure the low energy portion of the spectrum, from 50 keV to 2 MeV. These spectra both show good agreement with the current evaluation of ^{252}Cf and have low associated uncertainties providing a new high precision measurement that helps reduce the uncertainties in the prompt fission neutron spectrum for the spontaneous fission of ^{252}Cf.

DOI: 10.1103/PhysRevC.95.064615

I. INTRODUCTION

Accurate nuclear data is integral in several aspects of the nuclear field including reactor simulations, criticality safety, and stockpile stewardship [1]. One of the nuclear data quantities that has the highest associated uncertainties is the prompt fission neutron spectrum (PFNS). The most well-known and well-measured spectrum for PFNS is that of the spontaneous fission of ^{252}Cf. Because it's a spontaneous fission source, it is easier to measure the spectrum than for neutron induced fission reactions. Although it is considered a well-known spectrum, there are significant differences in the existing experimental data for the PFNS of ^{252}Cf. These can be seen in Fig. 1 and are most prevalent at the high energies, $E > 5$ MeV, and low energies, $E < 0.5$ MeV. These regions suffer from lower count rate, difficulty in neutron measurements because of short time of flight, and difficulty in γ neutron discrimination. Additionally, there are some discrepancies in the data sets and although the uncertainty on the evaluation is low, an additional measurement with uncertainties on the order of 5% will help improve the accuracy of the evaluation.

A greater understanding of the PFNS for ^{252}Cf is of significant interest for improving nuclear data. While ^{252}Cf has very little direct impact on nuclear reactor calculations, it can affect experimental nuclear data in two very key aspects. First, the PFNS of ^{252}Cf is often used to determine the efficiencies of neutron detectors [2]. Therefore, the accuracy of the efficiency measurements is only as good as the uncertainty on the ^{252}Cf PFNS. Additionally, many other PFNS such as ^{235}U and ^{239}Pu are often measured as a ratio to the ^{252}Cf spectrum [3]. This is advantageous because it minimizes systematic uncertainties in the data; however, it assumes a well-known spectrum for ^{252}Cf. The target uncertainty for the current measurement is below 5% which will provide a new more accurate measurement of the ^{252}Cf PFNS which will help reduce the uncertainties on the evaluation and provide a means for more accurate nuclear data from experiments to be obtained.

II. METHOD

A. Fission tagging

To determine the energy of the fission neutrons, the time-of-flight (ToF) method was utilized. This method determines the energy of the neutron through the relativistic kinetic energy equation given the distance the neutron traveled and the time it took for the neutron to travel the given distance. Equation (1) shows the relation between neutron ToF and neutron energy. In this equation m_n is the rest mass of the neutron given as 939.4943 MeV/c^2, t is the time of flight in seconds, c is the speed of light in a vacuum given as 2.99×10^8 m/s, and L is the flight-path distance in meters. With the fission source and detector at a fixed distance, the only variable becomes the time from the fission event to the neutron being recorded by the neutron detector. Traditionally, this was preformed using a fission chamber, measuring the energy deposition of the fission fragments. However, for this measurement the multiple γ tagging method was utilized, which takes advantage of the fission γ multiplicity on an array of γ detectors to determine when the fission event has occurred. This provides the timing for the fission event and was shown to accurately reproduce the (PFNS) [5]. While issues exist with single γ triggering because of delayed γ rays [6], the double coincidence using the multiple γ tagging method, with a 3-ns coincidence timing window, eliminates the false triggering on delayed γ rays. For this measurement a coincidence of two out of four γ detectors was used with a timing window of 3 ns between the events.

$$E(t) = m_n c^2 \left(\left(1 - \frac{L^2}{t^2 c^2} \right)^{-1/2} - 1 \right). \quad (1)$$

*blaine2@rpi.edu

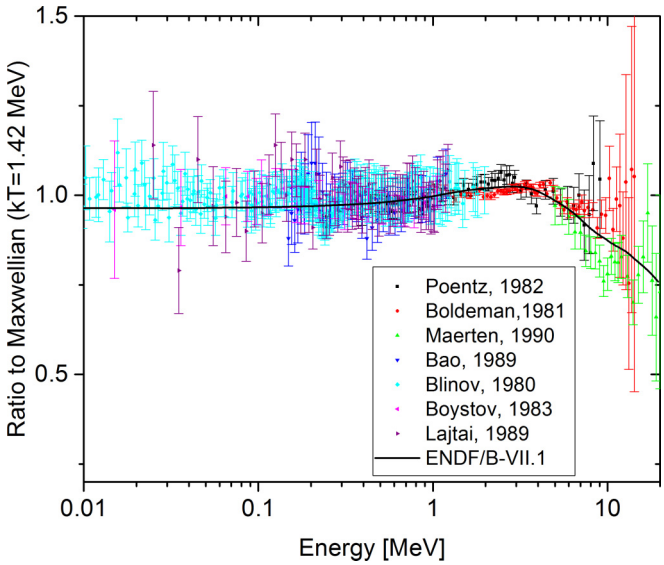

FIG. 1. A comparison of several measurements and uncertainties for the spontaneous fission of ^{252}Cf as well as the current ENDF/B-VII.1 [4] evaluation. The data sets are shown as a ratio to a Maxwellian distribution with the kT parameter of 1.42 MeV. This highlights the lack of experimental data below 0.5 MeV and above 7 MeV as well as the high uncertainties in the data sets.

B. Pulse shape discrimination

To separate neutron pulses from γ pulses on the EJ-301 liquid scintillator, a pulse shape analysis (PSA) method was used. This method relies on comparing the incident pulses to reference neutron and γ pulse shape and performing a least squares fit of the unknown pulse to the reference pulses. This will categorize the unknown pulse as either a neutron or γ, depending on which reference pulse it fits best with. This method was previously used to discriminate neutron and γ pulses at RPI for neutron scattering measurements [8]. Additionally, a γ misclassification correction is performed to reduce the number of γ pulses erroneously classified as neutron pulses [8].

C. Efficiency determination

One of the difficulties with measuring the PFNS for the spontaneous fission of ^{252}Cf is that typically the efficiency of neutron detectors is determined using the ^{252}Cf spectrum. However, because the ^{252}Cf PFNS is the measured quantity, it cannot be used for determining efficiency. Therefore, a different method was devised at RPI to determine the detector efficiency. Neutron detectors were placed in the pulsed neutron beam generated from the RPI 60-MeV electron linear accelerator (LINAC). The count rate that was measured on the detector was the product of the neutron flux incident on the detector and the neutron detection efficiency. To determine the neutron flux, a ^{235}U fission chamber was placed in the beam at the same location. The counts for each ToF channel are given by Eq. (2), where ϕ_i is the neutron flux in ToF channel i, η_i is the neutron detector efficiency, $\sigma_{235}(E_i)$ is the ^{235}U fission cross section for the energy equivalent of channel i, N is the number density of ^{235}U in the fission chamber, Δt_i is the width of ToF channel i, trigs is the number of total LINAC triggers, and B_0 is the steady-state background counts at long ToF.

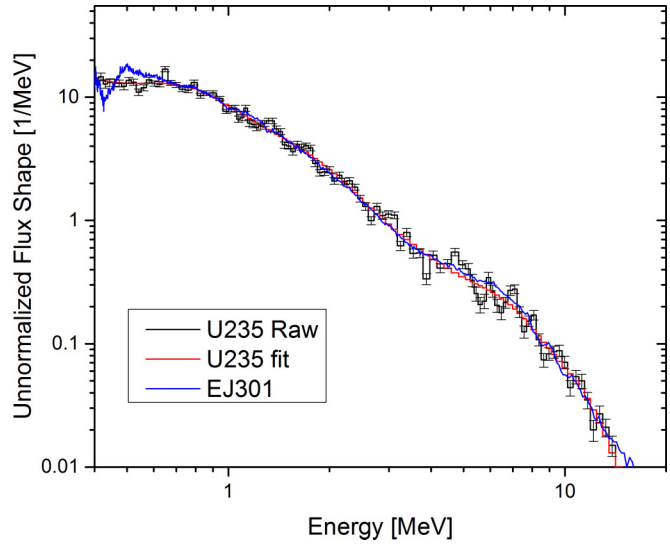

FIG. 2. The raw and smoothed flux measured with the ^{235}U fission chamber, and the flux found from direct measurement of the EJ-301 detector in beam.

$$C_i = N \cdot \phi_i \cdot \eta_i \cdot \bar{\sigma}_{235}(E_i) \cdot \Delta t_i \cdot \text{trigs} + B_0. \quad (2)$$

Because the ^{235}U fission cross section is a standard cross section [7], the neutron flux as a function of ToF can be determined. Additionally, the SCINFUL [9] code was utilized to predict the EJ-301 detector efficiency and generate a flux associated with the detector in beam measurement. Figure 2 shows the measured flux using the ^{235}U fission chamber compared to the flux calculated using the SCINFUL efficiencies. The raw data from the ^{235}U fission chamber was smoothed, using a seventh-order polynomial, to achieve the ^{235}U fit curve. In the overlap region from 0.7 to 4 MeV the EJ-301 determined flux agrees well with the ^{235}U determined flux to within 2%. This shows a good agreement between the flux obtained from the ^{235}U fission chamber and that calculated using the SCINFUL efficiencies.

III. EXPERIMENTAL SETUP

For this measurement a ^{252}Cf fission chamber was designed and fabricated at RPI containing 18.4 ng of Cf [5]. This fission chamber was used to compare the spectrum obtained with the fission chamber signal to that from the γ tagging method and was shown that both spectra show good agreement validating the γ tagging method [5]. While a larger sample could have been used, this sample size was sufficient for obtaining adequate statistics for the PFNS in the energy range from 50 keV to 7 MeV. The isotopic composition of the sample can be found in Table I. This sample resulted in a 9000 fission per second count rate with 99.7% being from the spontaneous fission of ^{252}Cf.

The detectors utilized in the experiment were four BaF_2 γ detectors, two EJ-301 liquid scintillators and one EJ-204 plastic scintillator. The BaF_2 detectors are hexagonal prisms

TABLE I. Isotopic composition of ^{252}Cf sample obtained from Oak Ridge National Laboratory. The assay was performed 6/30/2011.

Isotope	Atom percent	Weight percent
^{249}Cf	10.92	10.82
^{250}Cf	13.68	13.61
^{251}Cf	4.76	4.75
^{252}Cf	70.64	70.82

measuring 5 inches long and 2 inches across. The face of each detector was located 10 cm from the center of the fission sample in a square configuration with the detector centers located 10 inches apart. Each detector was surrounded by an 1/8-inch lead shield to prevent γ scattering between the detectors that can result in false coincidence events. The EJ-301 neutron detectors are 3-inch thick by 5-inch diameter and were placed 50 cm away from the center of the fission sample. This detector was used to measure the high energy portion of the PFNS, from 0.5 to 7 MeV. The EJ-204 detector was a 0.5-inch thick by 5-inch diameter detector and was located 48 cm away from the center of the fission sample. This detector was used to measure the low energy portion of the PFNS, from 50 keV to 2 MeV. The experimental setup for the system can be seen in Fig. 3.

All data was acquired in digital form using a set of four Acqiris 8-bit digital data acquisition boards. The boards were operated at a 1 giga-sample per second sampling rate corresponding to data being recorded at nanosecond intervals. The boards were operated in threshold mode with a pulse threshold of 195 millivolts corresponding to 80 keVee for the EJ-301 detector. The threshold was the same 195 millivolts for the EJ-204 detector, however, because it was operated at a much higher voltage it corresponds to 10 keVee. Each pulse was

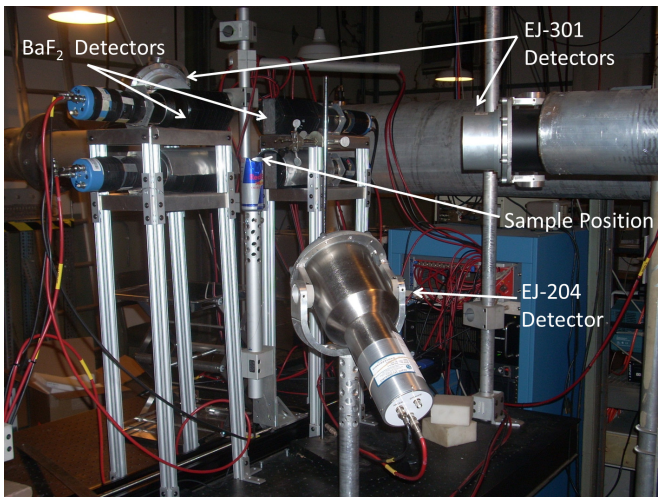

FIG. 3. The experimental setup utilized for the measurement highlighting the location of the ^{252}Cf fission chamber, the BaF_2 γ detectors, and the EJ-204 and EJ-301 neutron detectors. The γ detectors are located 10 cm away from the sample, the EJ-301 detectors are located 50 cm away from the sample, and the EJ-204 detector is located 48 cm away from the sample.

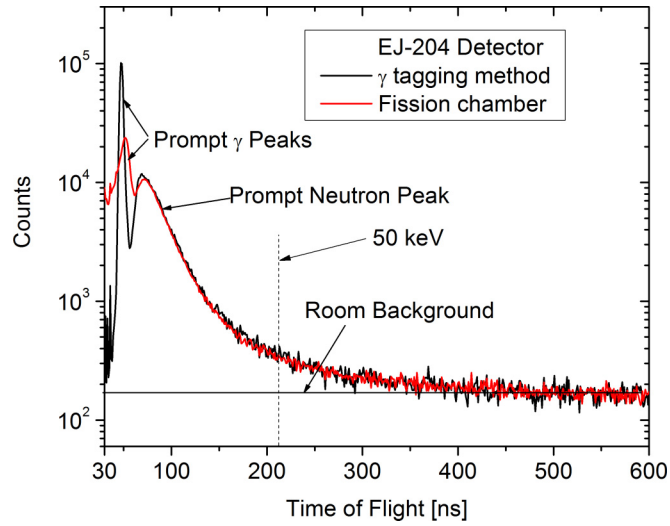

FIG. 4. The constant time-independent room background as seen as the average count rate from 500 to 600 ns after the fission event. The background continues to remain constant at longer time of flights.

recorded for a total of 120 ns with 16 ns before the pulse crosses the threshold and 104 seconds following. This allows for any dc offset present on the board to be subtracted from the pulse. The pulse data, including the detector number, timing, and full pulse information, was stored for post-processing analysis.

IV. RESULTS

A. Background

Once the data was converted into a ToF spectrum, the counts from background were subtracted. Three background components were characterized: time-independent background, time-dependent neutron background, and time-dependent γ background. The easiest of these to determine is the time-independent background that comes from random events not correlated with the fission process occurring in the measurement window. This can be seen visually in Fig. 4 where the count rate flattens out at long ToF and was determined by averaging the count rate per channel in the region from 500 to 600 ns and subtracting this value from each channel.

The second background component, the time-dependent γ background, comes primarily from the γ decay of fission fragments in metastable states. Usually the prompt fission γ's are released within a nanosecond after the fission event; however, some fission fragments are produced in metastable states which decay at longer times up to several microseconds [10]. This background is not present with the EJ-301 detector because PSA can be preformed to remove the γ's. However, because PSA cannot be performed on the EJ-204 detector, this background needs to be removed. To determine this component, the MCNP-POLIMI [11] code was used to model the background. However, the POLIMI code was found to overestimate the late prompt γ contribution. Therefore, a correction factor on the POLIMI simulations was determined to predict the γ background. Figure 5 shows a comparison of the simulated γ response of an EJ-301 detector in MCNP-POLIMI against the actual experimental measurement taken from an

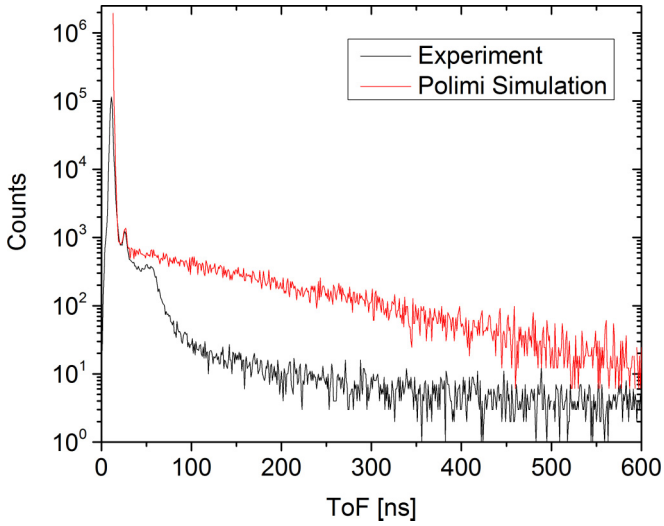

FIG. 5. A comparison of the measured γ signal from an EJ-301 detector using PSA to the simulated signal from MCNP-POLIMI. The spectra are normalized at the carbon scattering peak at 40 ns. This shows an increase in the simulated counts at longer ToFs.

experiment with ^{252}Cf. The spectra were normalized at the peak at 40 ns, which corresponds to high energy scattering off carbon in the detector. By taking a ratio of the counts from the measurement to the counts from the simulation, a correction factor was determined and applied to the simulation with EJ-204. This results in the time-dependent γ background correction for the EJ-204 detector as seen in Fig. 6. While the γ spectrum can be directly measured with either the BaF_2 or EJ-301 detectors, these detectors both have different efficiency and operate at a higher low energy discriminator threshold than the EJ-204 detector. Therefore, the most accurate method

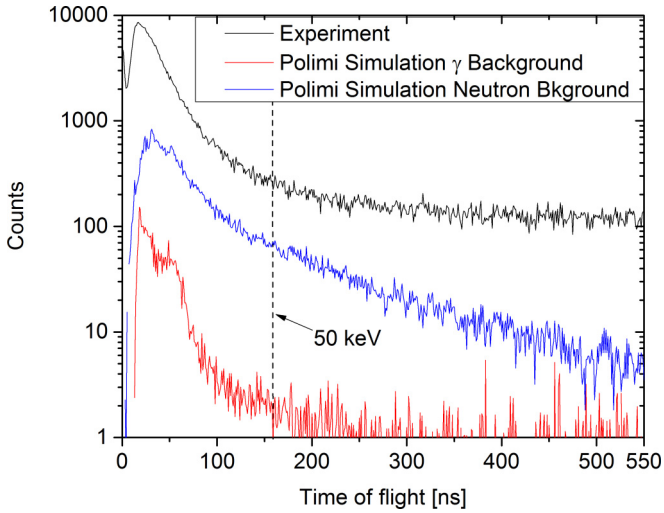

FIG. 6. The background components found using MCNP-POLIMI simulations for the EJ-204 plastic scintillation detector. The neutron background is found from simulating the neutron scattering off the surrounding materials and the γ background is from the decay of isomeric states. The 50-keV line is shown to signify where the experimental data ends for the PFNS measurement.

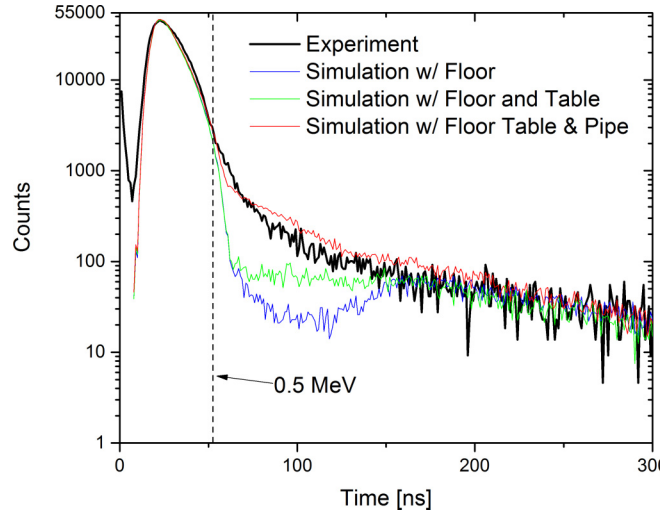

FIG. 7. The effects of neutron scattering in an MCNP-POLIMI simulation from several background materials. This shows that the floor, experiment table, and central flight tube need to be accurately modeled to predict the time-dependent neutron background for the experiment. The 0.5-MeV line shows the lower limit for the PFNS for the EJ-301 liquid scintillator.

for determining the time-dependent γ background is to scale the simulation based on the experimental measurement of the EJ-301 detector.

The third and final background component that was addressed is the time-dependent neutron background. This affects both the EJ-301 and EJ-204 detectors and is primarily from high energy prompt fission neutrons scattering off surrounding structure and scattering back to the neutron detectors. The fission rate from the sample was approximately 9000 fissions per second and was low enough that fission events were highly unlikely to cause significant neutron background. To determine the materials responsible for the neutron scattering background, an MCNP-POLIMI simulation was performed modeling different parts of the room including the experiment table, the floor, and the central flight tube.. The effects of each of these components can be seen in Fig. 7, and a diagram of the simulation is shown in Fig. 8. Additionally, the BaF_2 γ detectors were included in the background simulation and accounted for 2% of the total background. Once the background components were determined, a simulation was performed with and without the background, and the difference was found to be the neutron contribution from the background alone. This was then compared to the experiment and agrees very well with the signal at long ToFs, in the region from 100 to 300 ns. In this region only scattered neutrons are recorded by the experiment so this demonstrates that the simulation can accurately predict the scattered neutron background. Therefore, the POLIMI simulation was used to determine the time-dependent neutron background for the experiments and subtracted off. Figure 9 shows the comparison of the experiment and the time-dependent neutron background component. Once all of these background components were determined and subtracted from the experimental signal, it is in a form which can be converted from ToF to an energy spectrum.

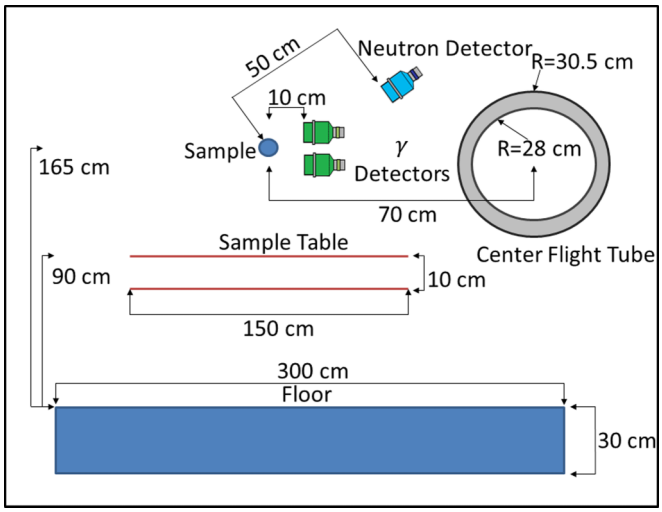

FIG. 8. A diagram (not to scale) showing a side view of the geometry used to model the MCNP-POLIMI simulations. The three primary sources of neutron scattering background: The experiment table, floor, and central flight tube are shown.

B. Data analysis

Once all of the background components and the efficiencies were determined the final ToF spectrum was obtained. The data is grouped into ToF bins where j is the ToF channel directly from the digital data and i corresponds the larger ToF bin. This data is corrected using Eq. (3), where $B1$, $B2$, and $B3$ are the time-independent background, time-dependent neutron background, and time-dependent γ background, respectively; C is the counts from the experiment, and η is the neutron detection efficiency for the larger ToF bin. The data is then converted from a time domain to an energy domain using Eq. (1) to yield the final PFNS. Figures 10 and 11 show the EJ-301 detector and EJ-204 detector, respectively. Also shown are a comparison to the current ENDF evaluation of the ^{252}Cf spontaneous fission PFNS along with several of the leading experimental data sets. For the high energy data in Fig. 10 the data sets were normalized to the ENDF evaluation at 1 MeV except for the Maerten data set which was normalized at 5 MeV. For the low energy data in Fig. 11 all data sets were normalized to

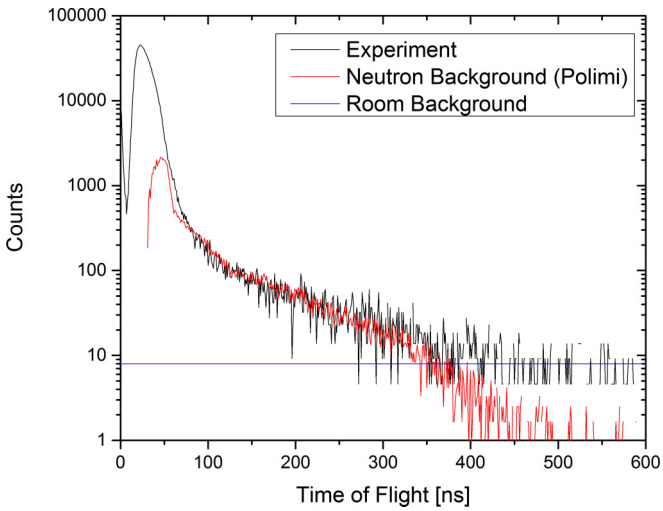

FIG. 9. A comparison of the experimental ToF PFNS for the EJ-301 liquid scintillator compared to the MCNP-POLIMI obtained neutron background. Also shown is the time-independent room background. This shows good agreement between the simulation and the experiment, from 100 to 300 ns, a region past the PFNS where only scattered background neutrons are present.

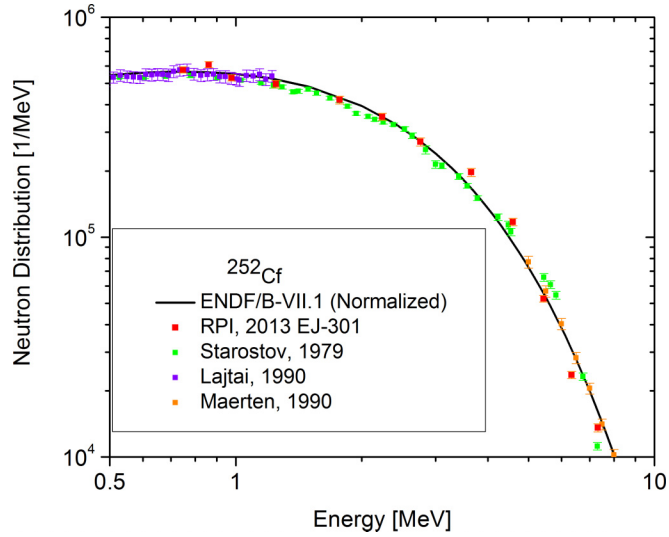

FIG. 10. The high energy portion of the ^{252}Cf spontaneous fission PFNS taken with an EJ-301 liquid scintillator in the region from 0.5 to 7 MeV. Also shown are the ENDF/B VII.1 evaluation and several prominent data sets showing good agreement between the RPI data and the current evaluations and data sets. The data sets were normalized to the ENDF evaluation at 1 MeV except for the Maerten data which was normalized at 5 MeV.

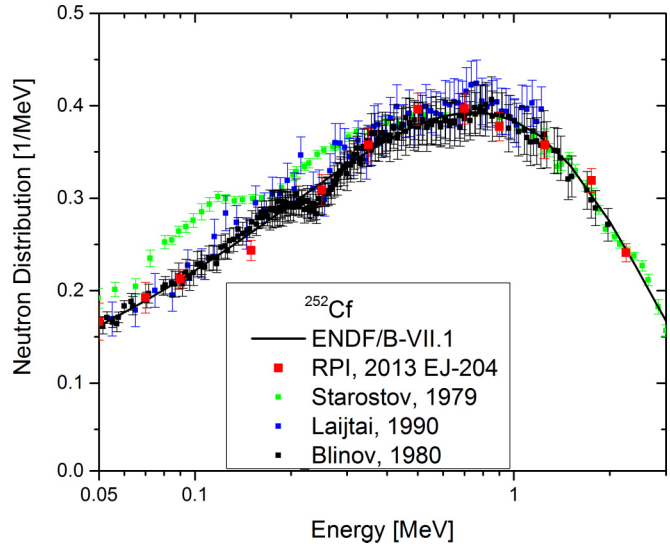

FIG. 11. The low energy portion of the ^{252}Cf spontaneous fission PFNS taken with an EJ-204 plastic scintillator in the region from 50 keV to 2 MeV. Also shown are the ENDF/B VII.1 evaluation and several prominent data sets showing good agreement between the RPI data and the current evaluations and data sets. The data sets were normalized to the ENDF evaluation at 1.2 MeV.

TABLE II. Tabulated data for PFNS measurement of spontaneous fission of ^{252}Cf using a multiple γ tagging method from 7.839 to 0.7 MeV found using 3-inch × 5-inch EJ-301 liquid scintillator. Here E1 and E2 are the start and end of the energy bin, respectively. The midpoint energy is found from the midpoint of the time bins not the energy bins.

E1 (MeV)	E2 (MeV)	Midpoint E (MeV)	Data (Counts)	Data uncertainty (%)
7.84	6.82	7.30	13 580	4.25
6.82	5.87	6.32	23 596	3.81
5.87	5.00	5.41	52 474	3.55
5.00	4.19	4.57	117 110	3.86
4.19	3.11	3.59	197 059	4.23
3.11	2.41	2.73	271 162	4.21
2.41	2.07	2.23	352 655	3.64
2.07	1.47	1.73	420 320	4.08
1.47	1.03	1.22	497 257	3.84
1.03	0.93	0.98	530 608	3.21
0.93	0.80	0.86	608 788	3.25
0.80	0.70	0.75	577 266	3.18

the ENDF evaluation at 1.2 MeV. These are primarily the data sets used in the evaluation by Manhart [12]. The new RPI data shown have very low uncertainties and agree very well with the previous evaluation. The tabulated data for the EJ-301 and EJ-204 detectors can be seen in Tables II and III, respectively.

$$D_i = \frac{\sum_{j=1}^{J}(C_j - B1_j - B2_j - B3_j)}{\eta_i \cdot \Delta E_i}. \tag{3}$$

C. Uncertainty

The uncertainty in the data was determined by propagating the uncertainties through Eq. (3) to obtain Eq. (4). Here σ_{Cj}^2 and σ_{B1j}^2 are determined simply as the square root of the counts using counting statistics. Because the time-dependent background components were found using the MCNP-POLIMI simulation, a different form of uncertainty needed to be applied. To determine the uncertainty for the time-dependent neutron background, the simulation was compared directly to the experimental data. Because the constant room background is not present in the simulation, it was first subtracted from the experimental data. The simulation was normalized to the experiment at the PFNS peak and a Chi-squared analysis was performed in the region from 70 to 120 ns. This region was selected because it was after the PFNS signal while still having significant background counts. This provides a systematic uncertainty for using the simulation to predict the time-dependent neutron and γ backgrounds.

$$\sigma_{Di} = D_i \left(\left(\frac{\sqrt{\sum_j^J \left(\sigma_{Cj}^2 + \sigma_{B1j}^2 + \sigma_{B2j}^2 + \sigma_{B3j}^2\right)}}{\sum_j^J (C_j - B1_j - B2_j - B3_j)} \right)^2 + \left(\frac{\sigma\eta_i}{\eta_i} \right)^2 \right)^{0.5}. \tag{4}$$

The final uncertainty which needs to be addressed is the uncertainty in the detector efficiency for both the EJ-301 and EJ-204 detectors. The uncertainty in the EJ-301 detector was found by comparing the flux shown in Fig. 2 for the ^{235}U fission chamber with the EJ-301 flux calculated using SCINFUL efficiencies with in-beam measurements. This allowed for individual detector efficiencies to be measured and compared with the fission chamber results. Because the EJ-204 detector suffers from high γ background when placed in an incident neutron beam, the exact detector efficiency cannot be obtained with this method and the SCINFUL code was used. The uncertainty for this efficiency was found by comparing the SCINFUL efficiency for the EJ-301 detector with that found using the fission chamber. This uncertainty was then applied to the EJ-204 SCINFUL efficiency.

TABLE III. Tabulated data for PFNS measurement of spontaneous fission of ^{252}Cf using a multiple γ tagging method from 2.8 to 0.05 MeV found using 0.5-inch × 5-inch EJ-204 liquid scintillator. Here E1 and E2 are the start and end of the energy bin, respectively.

E1 (MeV)	E2 (MeV)	Midpoint E (MeV)	Data (counts)	Data uncertainty (%)
3.10	2.57	2.82	275 361	4.02
2.57	2.06	2.29	418 419	4.05
2.06	1.54	1.77	553 682	4.02
1.54	1.03	1.25	620 531	4.09
1.03	0.82	0.92	655 040	4.06
0.82	0.62	0.71	688 850	4.20
0.62	0.41	0.50	687 659	4.42
0.41	0.31	0.35	620 518	5.07
0.31	0.21	0.25	536 094	5.37
0.21	0.11	0.14	422 739	4.50
0.11	0.085	0.095	369 298	4.70
0.085	0.063	0.073	333 909	8.59
0.063	0.042	0.051	289 043	12.10

V. CONCLUSIONS

The multiple γ tagging method was used to accurately measure the prompt fission neutron spectrum for the spontaneous fission of ^{252}Cf in the energy range from 50 keV to 7 MeV. The experimental uncertainties associated with the measurement are low and the experimental data shows good agreement with the previous evaluation by Manhart. This measurement can help reduce the uncertainties on the PFNS which is used in several aspects of nuclear data research including determining detector efficiency and measuring other fission neutron spectra as a ratio to ^{252}Cf.

ACKNOWLEDGMENTS

The authors express their appreciation to the LINAC staff for their expertise and diligent work. The authors also thank the Stewardship Science Academic Alliance for their funding of this research, Grants No. DE-FG52-09NA29453 and No. DE-NA0001814.

[1] A. Klein and J. Lance, *Future Directions, Challenges and Opportunities in Nuclear Energy*, Report No. INL/CON-06-11735 (Idaho National Lab, Idaho Falls, 2006).
[2] G. Knoll, *Radiation Detection and Measurement*, 3rd ed. (John Wiley and Sons, Hoboken, 2000).
[3] H. Werle and H. Bluhm, Fission-neutron spectra measurements of ^{235}U, ^{239}Pu and ^{252}Cf, J. Nucl. Energy **26**, 165 (1972).
[4] M. B. Chadwick *et al.*, ENDF/B-VII.1 Nuclear data for science and technology: Cross sections, covariances, fission product yields and decay data, Nuclear Data Sheets **112**, 2887 (2011).
[5] E. Blain, A. Daskalakis, R. C. Block, D. Barry, and Y. Danon, A method to measure prompt fission neutron spectrum using gamma multiplicity tagging, Nucl. Inst. Meth. Phys. Res. **805**, 95 (2016).
[6] T. Granier, Reanalysis of ^{239}Pu prompt fission neutron spectra, Phys. Procedia **64**, 183 (2015).
[7] A. Carlson *et al.*, International evaluation of neutron cross section standards, Nuclear Data Sheets **110**, 3215 (2009).
[8] A. M. Daskalakis *et al.*, Quasi-differential neutron scattering from ^{238}U from 0.5 to 20 MeV, Ann. Nucl. Energy **73**, 455 (2014).
[9] J. K. Dickens, SCINFUL - A Monte Carlo Based Computer Program to Determine a Scintillator Full Energy Response to Neutron Detection for E_n between 0.1 and 80 MeV: User's Manual and FORTRAN Program Listing, Report No. ORNL-6462 (Oak Ridge National Laboratory, Oak Ridge, 1988).
[10] C. Wagemans, *The Nuclear Fission Process* (CRC Press, Boca Raton, 1991).
[11] E. Padovani and S. A. Pozzi, MCNP-POLIMI User's Manual (Library of Nuclear Engr. Dept., Polytechnic of Milan, Italy, 2002).
[12] W. Mannhart, *Report No. IAEA-TECDOC-410* (International Atomic Energy Agency, Vienna, 1987).